

Non-Abelian statistics and topological quantum computation in 1D wire networks

Jason Alicea,^{1,2} Yuval Oreg,³ Gil Refael,¹ Felix von Oppen,⁴ and Matthew P. A. Fisher¹

¹*Department of Physics, California Institute of Technology, Pasadena, California 91125*

²*Department of Physics and Astronomy, University of California, Irvine, California 92697*

³*Department of Condensed Matter Physics, Weizmann Institute of Science, Rehovot, 76100, Israel*

⁴*Dahlem Center for Complex Quantum Systems and Fachbereich Physik, Freie Universität Berlin, 14195 Berlin, Germany*

(Dated: June 24, 2010)

Topological quantum computation provides an elegant way around decoherence, as one encodes quantum information in a non-local fashion that the environment finds difficult to corrupt. Here we introduce a surprising new topological quantum computation platform: *one-dimensional* semiconductor wire networks. Previous work^{1,2} provided a recipe for driving semiconducting wires into a topological phase supporting long-sought particles known as Majorana fermions that can store topologically protected quantum information. Majorana fermions in this setting can be transported, created, and fused by applying locally tunable gates to the wire. More importantly, we show that networks of such wires allow Majorana fermions to be meaningfully braided and that they exhibit non-Abelian statistics like vortices in a $p + ip$ superconductor. We propose simple experimental setups that allow for the Majorana fusion rules to be probed, along with more complex networks that allow for efficient exchange of arbitrary numbers of Majorana fermions. This work paves a new path forward in the field of topological quantum computation that benefits from physical transparency and experimental realism.

PACS numbers:

The experimental realization of a quantum computer ranks among the foremost outstanding problems in condensed matter physics, particularly in light of the revolutionary rewards the achievement of this goal promises. Typically, decoherence presents the primary obstacle to fabricating a scalable quantum computer. In this regard *topological* quantum computing holds considerable promise, as here one embeds quantum information in a non-local, intrinsically decoherence-free fashion^{3–5}. The core ideas can be illustrated with a toy model of a spinless, two-dimensional $p + ip$ superconductor. Vortices in such a state bind exotic particles known as Majorana fermions, which cost no energy and therefore generate a ground state degeneracy. Because of the Majoranas, vortices exhibit non-Abelian braiding statistics^{6,7}: adiabatically exchanging vortices noncommutatively transforms the system from one ground state to another. Quantum information encoded in this ground state space can be controllably manipulated by braiding operations—something the environment finds difficult to achieve.

Despite this scheme’s elegance, realizing suitable topological phases poses a serious challenge. Most effort has focused on the quantum Hall state at filling fraction^{6,8} $\nu = 5/2$, though this route appears daunting due to the plateau’s fragility⁹. Fortunately, we are in the midst of a paradigm shift wherein such topological phases of matter need no longer be *found* in solid state systems—rather, they can be *engineered*. Indeed, topological insulators^{10,11}, semiconductor heterostructures^{12,13}, non-centrosymmetric superconductors^{14–16}, and quantum Hall systems at integer plateau transitions¹⁷ can all be engineered into non-Abelian topological phases similar to a spinless $p + ip$ superconductor.

More recently, two groups^{1,2} recognized that topological superconductivity can be perhaps most easily engineered in *one-dimensional* semiconducting wires deposited on an s -wave superconductor. These proposals provide the first realistic experimental setting for Kitaev’s¹⁸ one-dimensional topo-

logical superconducting state. Remarkably, the ends of such wires support a localized, zero-energy Majorana fermion^{1,2,18}. Motivated by the exciting possibility of experimentally realizing this phase, we examine the prospect of exploiting one-dimensional semiconducting wires for topological quantum computation.

The suitability of one-dimensional wires for this purpose is by no means obvious. Topological quantum computation requires Majorana fermions to be transported, created, and fused, and also relies on their non-Abelian exchange statistics. The first three criteria can be implemented in a physically transparent fashion by applying independently tunable gates to the wire. Satisfying the last criterion, however, poses a more serious puzzle. Indeed, conventional wisdom holds that braiding statistics is ill-defined in one dimension, since particles must pass through one another at some point during the exchange. This problem can be surmounted by considering *networks* of one-dimensional wires, the simplest being the T-junction of Fig. 3. Even in such networks, however, non-Abelian statistics does not immediately follow as recognized by Wimmer *et al.*¹⁹ For example, in a two-dimensional $p + ip$ superconductor, vortices binding the Majoranas play an integral role in establishing non-Abelian statistics^{6,7}. We demonstrate that despite the absence of vortices in the wires, Majorana fermions in semiconducting wires exhibit non-Abelian statistics and transform under exchange exactly like vortices in a $p + ip$ superconductor.

We further propose experimental setups ranging from minimal circuits (involving one wire and a few gates) that can probe the Majorana fusion rules, to scalable networks that enable efficient exchange of many Majoranas. The ‘fractional Josephson effect’^{1,2,10,18,20}, along with Hassler *et al.*’s recent proposal²¹ enable readout of the topological qubits in this setting. The relative ease with which one-dimensional wires can be driven into a topological superconducting state, combined with the physical transparency of the manipulations, render

the setups discussed here extremely promising topological quantum computation platforms.

I. MAJORANA FERMIONS IN ‘SPINLESS’ p -WAVE SUPERCONDUCTING WIRES

We begin by discussing the physics of a single wire. Valuable intuition can be garnered from Kitaev’s toy model for a spinless, p -wave superconducting N -site chain¹⁸:

$$H = -\mu \sum_{x=1}^N c_x^\dagger c_x - \sum_{x=1}^{N-1} (t c_x^\dagger c_{x+1} + |\Delta| e^{i\phi} c_x c_{x+1} + h.c.) \quad (1)$$

where c_x is a spinless fermion operator and μ , $t > 0$, and $|\Delta| e^{i\phi}$ respectively denote the chemical potential, tunneling strength, and pairing potential. The bulk- and end-state structure becomes particularly transparent in the special case¹⁸ $\mu = 0$, $t = |\Delta|$. Here it is useful to express

$$c_x = \frac{1}{2} e^{-i\frac{\phi}{2}} (\gamma_{B,x} + i\gamma_{A,x}), \quad (2)$$

with $\gamma_{\alpha,x} = \gamma_{\alpha,x}^\dagger$ Majorana fermion operators satisfying $\{\gamma_{\alpha,x}, \gamma_{\alpha',x'}\} = 2\delta_{\alpha\alpha'}\delta_{xx'}$. These expressions expose the defining characteristics of Majorana fermions—they are their own antiparticle and constitute ‘half’ of an ordinary fermion. In this limit the Hamiltonian can be written as

$$H = -it \sum_{x=1}^{N-1} \gamma_{B,x} \gamma_{A,x+1}. \quad (3)$$

Consequently, $\gamma_{B,x}$ and $\gamma_{A,x+1}$ ‘fuse’ to form an ordinary fermion $d_x = (\gamma_{A,x+1} + i\gamma_{B,x})/2$ which costs energy $2t$, reflecting the wire’s bulk gap. Conspicuously absent from H , however, are $\gamma_{A,1}$ and $\gamma_{B,N}$, which represent end-Majorana modes. These can be combined into an ordinary zero-energy fermion $d_{\text{end}} = (\gamma_{A,1} + i\gamma_{B,N})/2$. Thus there are two degenerate ground states $|0\rangle$ and $|1\rangle = d_{\text{end}}^\dagger |0\rangle$, where $d_{\text{end}} |0\rangle = 0$, which serve as topologically protected qubit states. Figure 1(a) illustrates this physics pictorially.

Away from this special limit the Majorana end states no longer retain this simple form, but survive provided the bulk gap remains finite¹⁸. This occurs when $|\mu| < 2t$, where a partially filled band pairs. The bulk gap closes when $|\mu| = 2t$, and for larger $|\mu|$ a topologically trivial superconducting state without end Majoranas emerges. Here pairing occurs in either a fully occupied or vacant band.

Realizing Kitaev’s topological superconducting state experimentally requires a system which is effectively spinless—*i.e.*, exhibits one set of Fermi points—and p -wave pairs at the Fermi energy. Both criteria can be satisfied in a spin-orbit-coupled semiconducting wire deposited on an s -wave superconductor by applying a magnetic field^{1,2} [see Fig. 1(b)]. The simplest Hamiltonian describing such a wire reads

$$\mathcal{H} = \int dx \left[\psi_x^\dagger \left(-\frac{\hbar^2 \partial_x^2}{2m} - \mu - i\hbar u \hat{\mathbf{e}} \cdot \boldsymbol{\sigma} \partial_x - \frac{g\mu_B B_z}{2} \sigma^z \right) \psi_x + (|\Delta| e^{i\phi} \psi_{\downarrow x} \psi_{\uparrow x} + h.c.) \right]. \quad (4)$$

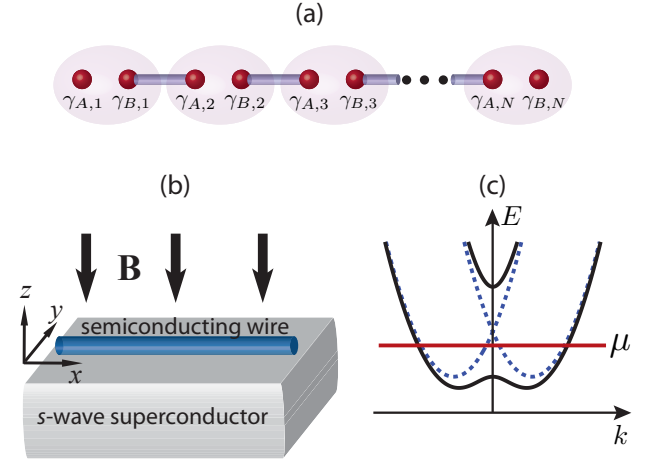


FIG. 1: (a) Pictorial representation of the ground state of Eq. (1) in the limit $\mu = 0$, $t = |\Delta|$. Each spinless fermion in the chain is decomposed in terms of two Majorana fermions $\gamma_{A,x}$ and $\gamma_{B,x}$. Majoranas $\gamma_{B,x}$ and $\gamma_{A,x+1}$ pair up to form an ordinary, finite energy fermion, leaving two zero-energy end Majoranas $\gamma_{A,1}$ and $\gamma_{B,N}$ as shown¹⁸. (b) A spin-orbit-coupled semiconducting wire deposited on an s -wave superconductor can be driven into a topological superconducting state exhibiting such end Majorana modes by applying an external magnetic field^{1,2}. (c) Band structure of the semiconducting wire when $\mathbf{B} = 0$ (dashed lines) and $\mathbf{B} \neq 0$ (solid lines). When μ lies in the band gap generated by the field, pairing inherited from the proximate superconductor drives the wire into the topological state.

The operator $\psi_{\alpha x}$ corresponds to electrons with spin α , effective mass m , and chemical potential μ . (We suppress the spin indices except in the pairing term.) In the third term, u denotes the (Dresselhaus²² and/or Rashba²³) spin-orbit strength, and $\boldsymbol{\sigma} = (\sigma^x, \sigma^y, \sigma^z)$ is a vector of Pauli matrices. This coupling favors aligning spins along or against the unit vector $\hat{\mathbf{e}}$, which we assume lies in the (x, y) plane. The fourth term represents the Zeeman coupling due to the magnetic field $B_z < 0$. Note that spin-orbit enhancement can lead to²⁴ $g \gg 2$. Finally, the last term reflects the spin-singlet pairing inherited from the s -wave superconductor via the proximity effect.

To understand the physics of Eq. (4), consider first $B_z = \Delta = 0$. The dashed lines in Fig. 1(c) illustrate the band structure here—clearly no ‘spinless’ regime is possible. Introducing a magnetic field generates a band gap $\propto |B_z|$ at zero momentum as the solid line in Fig. 1(c) depicts. When μ lies inside of this gap the system exhibits only a single pair of Fermi points as desired. Turning on Δ which is weak compared to the gap then effectively p -wave pairs fermions in the lower band with momentum k and $-k$, driving the wire into Kitaev’s topological phase^{1,2}. [Singlet pairing in Eq. (4) generates p -wave pairing because spin-orbit coupling favors opposite spins for k and $-k$ states in the lower band.] Quantitatively, realizing the topological phase requires^{1,2} $|\Delta| < g\mu_B |B_z|/2$, which we hereafter assume holds. The opposite limit $|\Delta| > g\mu_B |B_z|/2$ effectively violates the ‘spinless’ criterion since pairing strongly intermixes states from the upper band, producing an ordinary superconductor without Majorana modes.

In the topological phase, the connection to Eq. (1) becomes more explicit when $g\mu_B|B_z| \gg mu^2, |\Delta|$ where the spins nearly polarize. One can then project Eq. (4) onto a simpler one-band problem by writing $\psi_{\uparrow x} \sim \frac{u(e_y + ie_x)}{g\mu_B|B_z|} \partial_x \Psi_x$ and $\psi_{\downarrow x} \sim \Psi_x$, with Ψ_x the lower-band fermion operator. To leading order, one obtains

$$\mathcal{H}_{\text{eff}} \sim \int dx \left[\Psi_x^\dagger \left(-\frac{\hbar^2 \partial_x^2}{2m} - \mu_{\text{eff}} \right) \Psi_x + (|\Delta_{\text{eff}}| e^{i\varphi_{\text{eff}}} \Psi_x \partial_x \Psi_x + h.c.) \right], \quad (5)$$

where $\mu_{\text{eff}} = \mu + g\mu_B|B_z|/2$ and the effective p -wave pair field reads

$$|\Delta_{\text{eff}}| e^{i\varphi_{\text{eff}}} \approx \frac{u|\Delta|}{g\mu_B|B_z|} e^{i\varphi} (e_y + ie_x). \quad (6)$$

The dependence of φ_{eff} on \hat{e} will be important below when we consider networks of wires. Equation (5) constitutes an effective low-energy Hamiltonian for Kitaev's model in Eq. (1) in the low-density limit. From this perspective, the existence of end-Majoranas in the semiconducting wire becomes manifest. We exploit this correspondence below when addressing universal properties such as braiding statistics, which must be shared by the topological phases described by Eq. (4) and the simpler lattice model, Eq. (1).

We now seek a practical method to manipulate Majorana fermions in the wire. As motivation, consider applying a gate voltage to adjust μ uniformly across the wire. The excitation gap obtained from Eq. (4) at $k = 0$ varies with μ via

$$E_{\text{gap}}(k = 0) = \left| \frac{g\mu_B|B_z|}{2} - \sqrt{|\Delta|^2 + \mu^2} \right|. \quad (7)$$

For $|\mu| < \mu_c = \sqrt{(g\mu_B B_z/2)^2 - |\Delta|^2}$ the topological phase with end Majoranas emerges, while for $|\mu| > \mu_c$ a topologically trivial phase appears. Applying a gate voltage uniformly thus allows one to create or remove the Majorana fermions. However, when $|\mu| = \mu_c$ the bulk gap closes, and the excitation spectrum at small momentum behaves as $E_{\text{gap}}(k) \approx \hbar v |k|$, with velocity $v = 2u|\Delta|/(g\mu_B|B_z|)$. The gap closure is clearly undesirable, since we would like to manipulate Majorana fermions without generating additional quasiparticles.

This problem can be circumvented by employing a ‘keyboard’ of locally tunable gates as shown in Fig. 2, each of which impacts μ over a finite length L_{gate} of the wire. When a given gate locally tunes the chemical potential across $|\mu| = \mu_c$, a finite excitation gap $E_{\text{gap}} \sim \hbar v \pi / L_{\text{gate}}$ remains due to quantum confinement effects. Assuming $g\mu_B|B_z|/2 \sim 2|\Delta|$ and $\hbar u \sim 0.1\text{eV}\text{\AA}$ yields a velocity $v \sim 10^4\text{m/s}$; the gap for a $0.1\mu\text{m}$ wide gate is then of order 1K. We consider this a conservative estimate—heavy-element wires such as InSb and/or narrower gates could generate substantially larger gaps.

Local gates allow Majorana fermions to be transported, created, and fused. For instance, sequentially applying the leftmost gates in Fig. 2(a) drives the left end of the wire into an ordinary superconducting region, thereby transporting γ_1 rightward as in Fig. 2(b). Applying gates to nucleate a topological

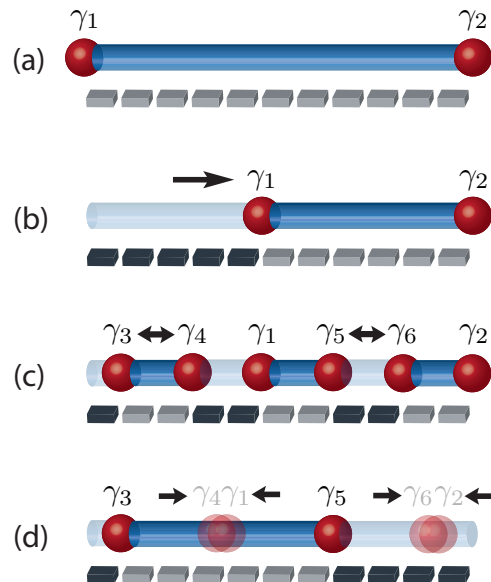


FIG. 2: Applying a ‘keyboard’ of individually tunable gates to the wire allows one to locally control which regions are topological (dark blue) and non-topological (light blue), and hence manipulate Majorana fermions while maintaining the bulk gap. This method allows Majorana fermions to be transported [(a)→(b)], created in pairs [(b)→(c)], and fused [(c)→(d)].

section of the wire from an ordinary region or vice versa creates pairs of Majorana fermions out of the vacuum; see Fig. 2(c). Similarly, removing a topological region entirely or connecting two topological regions fuses Majorana fermions as sketched in Fig. 2(d). In either case, a pair of Majorana end states strongly overlaps in the process and thus combines into an ordinary, finite-energy fermion.

As one germinates pairs of Majorana fermions, the ground state degeneracy increases as does our capacity to topologically store quantum information in the wire. Specifically, $2n$ Majoranas generate n ordinary zero-energy fermions whose occupation numbers specify topological qubit states. Manipulating these qubits, however, requires adiabatically braiding Majorana fermions, which is not possible in a single wire. Thus we now turn to the simplest arrangement which allows for exchange—the T-junction of Fig. 3.

II. MAJORANA BRAIDING AND NON-ABELIAN STATISTICS

First, we explore the physics at the junction where the wires in Fig. 3 meet (see the Supplementary Material for a more detailed discussion). It will be useful to view the T-junction as composed of three segments whose ends meet at a point. When only one segment realizes a topological phase, a single zero-energy Majorana fermion exists at the junction. When two topological segments meet at the junction, as in Figs. 3(a) and (b), generically no Majorana modes exist there. To see this, imagine decoupling the two topological segments so that two Majorana modes in close proximity exist at the junction;

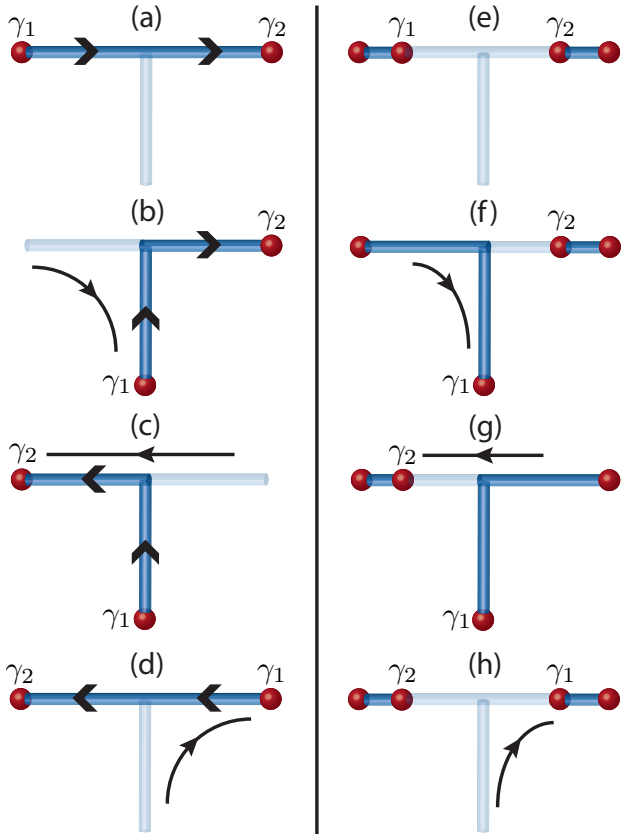


FIG. 3: A T-junction allows for adiabatic exchange of two Majorana fermions bridged by either a topological region (dark blue lines) as in (a)-(d), or a non-topological region (light blue lines) as in (e)-(h). Transport of Majorana fermions is achieved by gates as outlined in Fig. 2. The arrows along the topological regions in (a)-(d) are useful for understanding the non-Abelian statistics as outlined in the main text.

restoring the coupling generically fuses these Majoranas into an ordinary, finite-energy state.

As an illustrative example, consider the setup of Fig. 3(a) and model the left and right topological segments by Kitaev's model with $\mu = 0$ and $t = |\Delta|$ in Eq. (1). [For simplicity we will exclude the non-topological vertical wire in Fig. 3(a).] Suppose the superconducting phases are $\phi_{L/R}$ in the left/right chains and that the fermion $c_{L,N}$ at site N of the left chain couples weakly to the fermion $c_{R,1}$ at site 1 of the right chain via $H_{\Gamma} = -\Gamma(c_{L,N}^{\dagger}c_{R,1} + h.c.)$. Using Eq. (2), the end Majoranas at the junction couple as follows,

$$H_{\Gamma} \sim -\frac{i\Gamma}{2} \cos\left(\frac{\phi_L - \phi_R}{2}\right) \gamma_{B,N}^L \gamma_{A,1}^R \quad (8)$$

and therefore generally fuse into an ordinary fermion¹⁸. An exception occurs when the regions form a π -junction—that is, when $\phi_L - \phi_R = \pi$ —which fine-tunes their coupling to zero. Importantly, coupling between end Majoranas in the semiconductor context is governed by the same $\phi_L - \phi_R$ dependence as in Eq. (8)^{1,2}.

Finally, when all three segments are topological, again only

a single Majorana mode exists at the junction without fine-tuning. Three Majorana modes appear only when all pairs of wires simultaneously form mutual π junctions. Recall from Eq. (6) that the spin-orientation favored by spin-orbit coupling determines the effective superconducting phase of the semiconducting wires. Two wires at right angles to one another therefore exhibit a phase difference of $\pi/2$, well away from the pathological limits mentioned above.

The T-junction permits two types of (topologically equivalent) exchanges. First, consider the configuration of Fig. 3(a) where the horizontal wire resides in a topological phase while the vertical wire is non-topological. Counterclockwise exchange of γ_1 and γ_2 can be implemented as outlined in Figs. 3(b)-(d). Here, one shuttles γ_1 to the junction by making the left end non-topological; transports γ_1 downward by driving the vertical wire into a topological phase; transports γ_2 leftward in a similar fashion; and finally directs γ_1 up and to the right. Exchange of two Majorana fermions connected by a non-topological region as in Fig. 3(e) can be similarly achieved—counterclockwise exchange of γ_1 and γ_2 proceeds as sketched in Figs. 3(f)-(h).

While the Majoranas can now be exchanged, non-Abelian statistics is not obvious in this context. Recall how non-Abelian statistics of vortices arises in a spinless two-dimensional $p + ip$ superconductor^{6,7}, following Ivanov's approach. Ultimately, this can be deduced by considering two vortices which bind Majorana fermions γ_1 and γ_2 . Since the spinless fermion operators effectively change sign upon advancing the superconducting phase by 2π , one introduces branch cuts emanating from the vortices; crucially, a Majorana fermion changes sign whenever crossing such a cut. Upon exchanging the vortices, γ_2 (say) crosses the branch cut emanating from the other vortex, leading to the transformation rule $\gamma_1 \rightarrow \gamma_2$ and $\gamma_2 \rightarrow -\gamma_1$ which is generated by the unitary operator $U_{12} = \exp(\pi\gamma_2\gamma_1/4)$. With many vortices, the analogous unitary operators U_{ij} corresponding to the exchange of γ_i and γ_j do not generally commute, implying non-Abelian statistics.

Following an approach similar to that of Stern *et al.*²⁵, we now argue that Majorana fermions in semiconducting wires transform exactly like those bound to vortices under exchange, and hence also exhibit non-Abelian statistics. This can be established most simply by considering the exchange of two Majorana fermions γ_1 and γ_2 as illustrated in Figs. 3(a)-(d). At each step of the exchange, there are two degenerate ground states $|0\rangle$ and $|1\rangle = f^{\dagger}|0\rangle$, where $f = (\gamma_1 + i\gamma_2)/2$ annihilates $|0\rangle$. In principle, one can deduce the transformation rule from the Berry phases $\chi_n \equiv \text{Im} \int dt \langle n | \partial_t | n \rangle$ acquired by the ground states $|n\rangle = |0\rangle$ and $|1\rangle$, though in practice these are hard to evaluate.

Since exchange statistics is a universal property, however, we are free to deform the problem to our convenience provided the energy gap remains finite. As a first simplification, since the semiconductor Hamiltonian and Kitaev's model in Eq. (1) can be smoothly connected, let us consider the case where each wire in the T-junction is described by the latter. More importantly, we further deform Kitaev's Hamiltonian to be *purely real* as we exchange $\gamma_{1,2}$. The states $|0\rangle$ and $|1\rangle$

can then also be chosen real, leading to an enormous simplification: while these states still evolve nontrivially *the Berry phase accumulated during this evolution vanishes*.

For concreteness, we deform the Hamiltonian such that $\mu < 0$ and $t = \Delta = 0$ in the non-topological regions of Fig. 3. For the topological segments, reality implies that the superconducting phases must be either 0 or π . It is useful to visualize the sign choice for the pairing with arrows as in Fig. 3. (To be concrete, we take the pairing $|\Delta|e^{i\phi}c_jc_{j+1}$ such that the site indices increase moving rightward/upward in the horizontal/vertical wires; the case $\phi = 0$ then corresponds to rightward/upward arrows, while leftward/downward arrows indicate $\phi = \pi$.) To avoid generating π junctions, when two topological segments meet at the junction, one arrow must point into the junction while the other must point out. With this simple rule in mind, we see in Fig. 3 that although we can successfully swap the Majoranas while keeping the Hamiltonian real, we inevitably end up reversing the arrows along the topological region. In other words, the sign of the pairing has flipped relative to our initial Hamiltonian.

To complete the exchange then, we must perform a gauge transformation which restores the Hamiltonian to its original form. This can be accomplished by multiplying all fermion creation operators by i ; in particular, $f^\dagger = (\gamma_1 - i\gamma_2)/2 \rightarrow if^\dagger = (\gamma_2 + i\gamma_1)/2$. It follows that $\gamma_1 \rightarrow \gamma_2$ and $\gamma_2 \rightarrow -\gamma_1$, which is generated by the unitary transformation $U_{12} = \exp(\pi\gamma_2\gamma_1/4)$ exactly as in the $p + ip$ case discussed above. Note that the second type of braiding exhibited in Figs. 3(e)-(h) is topologically equivalent to the first, so that our results apply to this case as well. In the situation where many Majoranas are present in the wires, pairwise exchanges are implemented by analogous unitary operators U_{ij} , which again do not generally commute with one another. Thus the statistics is non-Abelian as advertised. In the Supplementary Material, we further bolster these results by conducting a complementary analysis which explicitly analyzes the wavefunctions $|0\rangle$ and $|1\rangle$ in a tractable limit; additionally, we similarly examine exchange of the type shown in Figs. 3(e)-(h) in a simple exactly solvable model yielding four Majorana modes.

III. DISCUSSION

The keyboard of gates shown in Fig. 2 and the T-junction of Fig. 3 provide the basic elements required to manipulate topological qubits in semiconducting wires. In principle, a single T-junction can support numerous well-separated Majorana modes, each of which can be exchanged with any other. (First, create many Majoranas in the horizontal wire of the T-junction. To exchange a given pair, shuttle all intervening Majoranas down to the end of the vertical wire and then carry out the exchange using the methods of Fig. 3.) However, networks consisting of several T-junctions—such as the setup of Fig. 4(a)—enable more efficient Majorana exchange. In the figure, all adjacent Majorana fermions can be immediately swapped using Fig. 3, while non-adjacent Majoranas can be shuttled down to the lower wire to be exchanged. This ‘ladder’ configuration straightforwardly scales up by introducing

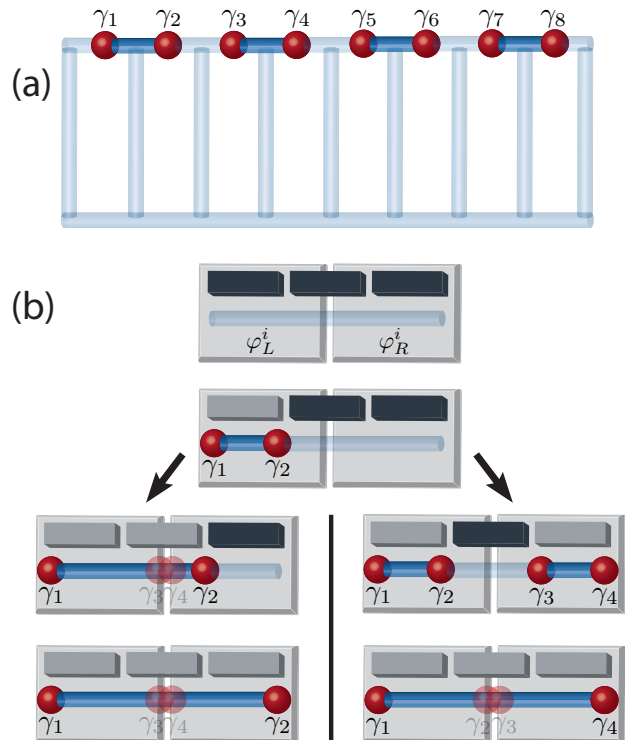


FIG. 4: (a) Example of a semiconductor wire network which allows for efficient exchange of many Majorana fermions. Adjacent Majoranas can be exchanged as in Fig. 3, while non-adjacent Majoranas can be transported to the lower wire to be similarly exchanged. (b) Minimal setup designed to detect the non-trivial Majorana fusion rules. Majoranas $\gamma_{1,2}$ are first created out of the vacuum. In the left path, γ_2 is shuttled rightward, and Majoranas $\gamma_{3,4}$ always fuse into a finite-energy state which is unoccupied. In the right path, $\gamma_{3,4}$ are also created out of the vacuum, and then γ_2 and γ_3 fuse, creating an extra occupied quasiparticle at the junction with 50% probability. The Josephson current flowing across the junction allows one to deduce the presence or absence of this extra quasiparticle.

additional ‘rungs’ and/or ‘legs’.

As Fu and Kane¹⁰ suggested, fusing Majorana fermions across a Josephson junction provides a readout method for the topological qubit states. We illustrate the physics with the schematic setup of Fig. 4(b), which extends the experiments proposed in Refs. 1,2 to allow the Majorana fusion rules to be directly probed. Here a semiconducting wire bridges two s -wave superconductors with initial phases $\varphi_{L/R}^i$; we assume $\Delta\varphi^i \equiv \varphi_L^i - \varphi_R^i \neq \pi$. Three gates drive the wire from an initially non-topological ground state into a topological phase. Importantly, the order in which one applies these gates qualitatively affects the physics. As we now discuss, only in the left path of Fig. 4(b) can the qubit state at the junction be determined in a single measurement.

Consider first germinating Majorana fermions γ_1 and γ_2 by applying the left gate. Assuming $f_A = (\gamma_1 + i\gamma_2)/2$ initially costs finite energy as γ_1 and γ_2 separate, the system will be prepared into a ground state with f_A unoccupied. Applying the central and then right gates shuttles γ_2 to the other end [see the left path of Fig. 4(b)]. Since a narrow insulat-

ing barrier separates the superconductors, an ordinary fermion $f_B = (\gamma_3 + i\gamma_4)/2$ arises from two fused Majoranas $\gamma_{3,4}$ at the junction. Similar to Eq. (8), the energy of this mode is well-captured by^{1,2,18} $H_J \sim i\epsilon^i \gamma_3 \gamma_4 = \epsilon^i (2f_B^\dagger f_B - 1)$ where $\epsilon^i = \delta \cos(\Delta\varphi^i/2)$ with non-universal δ . The system has been prepared in a ground state, so the f_B fermion will be absent if $\epsilon^i > 0$ but occupied otherwise.

Suppose we now vary the phase difference across the junction away from its initial value to $\Delta\varphi$. The measured Josephson current (see Supplementary Material for a pedagogical derivation) will then be

$$I = \frac{2e}{\hbar} \frac{dE}{d\Delta\varphi} = \frac{e\delta}{\hbar} \text{sgn}(\epsilon^i) \sin(\Delta\varphi/2) + I_{2e}, \quad (9)$$

where E is the ground-state energy and I_{2e} denotes the usual Cooper-pair-tunneling contribution. The first term on the right reflects single-electron tunneling originating from the fused Majoranas $\gamma_{3,4}$. This ‘fractional’ Josephson current exhibits 4π periodicity in $\Delta\varphi$, but 2π periodicity in the initial phase difference $\Delta\varphi^i$.

The right path in Fig. 4(b) yields very different results, reflecting the nontrivial Majorana fusion rules. Here, after creating $\gamma_{1,2}$ one applies the rightmost gate to nucleate another pair $\gamma_{3,4}$. Assuming f_A and f_B defined as above initially cost finite energy, the system initializes into the ground state $|0, 0\rangle$ satisfying $f_{A/B}|0, 0\rangle = 0$. Applying the central gate then fuses γ_2 and γ_3 at the junction. To understand the outcome, it is useful to re-express the ground state in terms of $f'_A = (\gamma_1 + i\gamma_4)/2$ and $f'_B = (\gamma_2 + i\gamma_3)/2$. In this basis $|0, 0\rangle = (|0', 0'\rangle - i|1', 1'\rangle)/\sqrt{2}$, where $f'_{A,B}$ annihilate $|0', 0'\rangle$ and $|1', 1'\rangle = f'_A f'_B |0', 0'\rangle$. Following our previous discussion, f'_B acquires finite energy at the junction, lifting the degeneracy between $|0', 0'\rangle$ and $|1', 1'\rangle$. Measuring the Josephson current then collapses the wavefunction with 50% probability onto either the ground state, or an excited state with an extra quasiparticle localized at the junction. In the former case Eq. (9) again describes the current, while in the latter the fractional contribution simply changes sign.

In more complex networks such as that of Fig. 4(a), fusing the Majoranas across a Josephson junction—and in particular measuring the sign of the fractional Josephson current—similarly allows qubit readout. Alternatively, the interesting recent proposal of Hassler *et al.*²¹ for reading qubit states via ancillary non-topological flux qubits can be adapted to these setups (and indeed was originally discussed in terms of an isolated semiconducting wire²¹).

To conclude, we have expanded the growing number of topological quantum computation arenas to include a surprising new entry—networks of *one-dimensional* semiconducting wires. From a fundamental standpoint, realizing non-Abelian statistics in this setting is quite remarkable. Perhaps even more appealing, however, are our proposal’s physical transparency and experimental promise, particularly given the feats already achieved in Ref. 26. While topological quantum computation in wire networks requires much experimental progress, observing the distinct fusion channels characteristic of the two paths of Fig. 4(b) would provide a remarkable

step en route to this goal. Finally, extending our proposal to enable *universal* quantum computation^{5,27,28} presents an extremely important open issue.

IV. SUPPLEMENTARY MATERIAL

A. Properties of the T-junction

Here we investigate in greater detail the properties of the junction in Fig. 3 where the three wire segments meet. There are three cases to consider, corresponding to the situations where one, two, or all three of the wire segments emanating from the junction reside in a topological superconducting state. It is conceptually simplest to address each case by viewing the T-junction as composed of three independent wire segments as in Fig. 5, which initially decouple from one another. In this limit a single Majorana exists at the end of each topological segment. One can then straightforwardly couple the wire segments at the junction and explore the fate of the Majorana end states.

Suppose that the phases of the p -wave pair fields in each region are $\phi_{A/B/C}$ as shown in Fig. 5 [in the semiconductor wire context, these phases correspond to φ_{eff} in Eq. (6)]. To be precise, if the wires are described by a lattice model, we define these phases relative to a pairing term $|\Delta|e^{i\phi_\alpha} c_j c_{j+1}$ such that the site indices increase moving rightward in the horizontal wires and upward in the vertical wire. A similar convention can be employed in the semiconductor wire context. Now suppose we allow single-electron tunneling between the ends of each segment, with amplitude Γ as shown schematically in Fig. 5. (Pairing between electrons residing at the ends of each region is also generally allowed, but does not change any qualitative results below and will therefore be neglected.) For convenience we will assume that the tunneling strength is weak compared to the bulk gaps in the wires, which will allow us to focus solely on the Majorana end states; our conclusions, however, are more general and do not require this assumption.

In the setup of Fig. 5(a) with only one topological region, the Majorana γ_1 is qualitatively unaffected by the coupling to the non-topological wires. At most its wavefunction can be quantitatively modified, but it necessarily remains at zero energy. This reflects the familiar topological protection of a single isolated Majorana mode in a gapped system.

With two of the three wires topological as in Fig. 5(b), the end Majoranas γ_1 and γ_2 generally fuse into an ordinary finite-energy fermion, except with fine-tuning. To a good approximation, the Majoranas couple through a Hamiltonian^{1,2,18}

$$H_{12} \propto -i\Gamma \cos\left(\frac{\phi_A - \phi_B}{2}\right) \gamma_1 \gamma_2. \quad (10)$$

This was discussed in the main text in the context of two wires described by Kitaev’s toy model in a particular limit, but is qualitatively rather general—the 4π periodicity in $\phi_A - \phi_B$ has a topological origin¹⁸. For instance, end Majoranas in two topological semiconducting wires coupled through an ordinary region exhibit the same phase dependence as above^{1,2}.

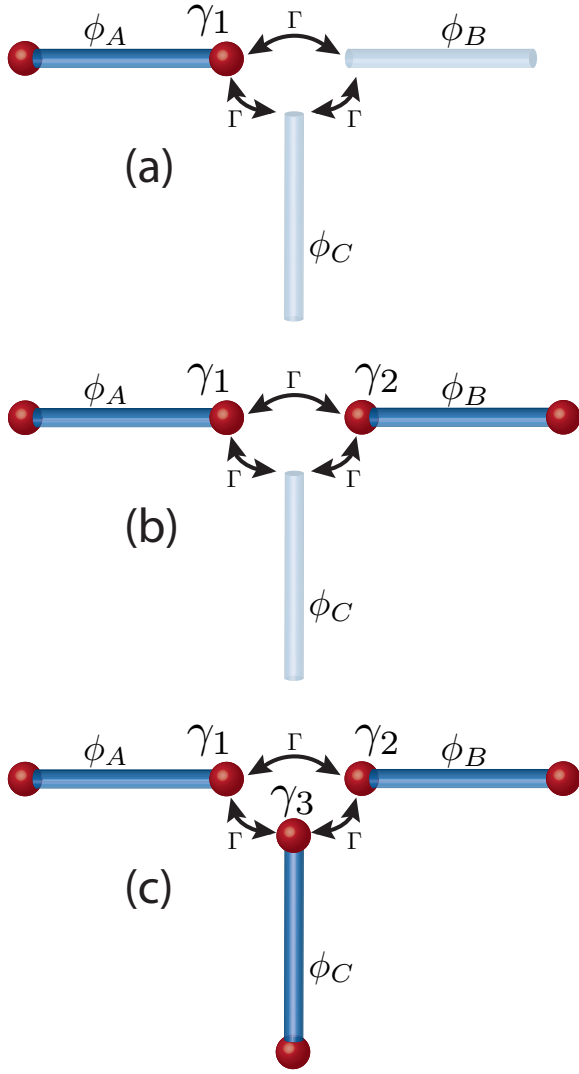


FIG. 5: T-junction viewed as three wire segments with p -wave superconducting phases $\phi_{A,B,C}$. The ends of each segment are coupled via tunneling with amplitude Γ as shown. (a) When only one segment is topological, the tunneling can not destroy the Majorana γ_1 at the junction. (b) Two topological regions meeting at the junction leads to the end Majoranas γ_1 and γ_2 generally fusing to an ordinary, finite-energy fermion, unless the topological wires form a π junction. (c) When all the three wires are topological, the Majoranas $\gamma_{1,2,3}$ generally fuse to form a finite-energy fermion and a single topologically protected Majorana. All three Majoranas remain at zero energy only when all three wire segments form mutual π junctions.

Equation (10) demonstrates that γ_1 and γ_2 remain zero-energy modes only when the topological wires form a π junction, *i.e.*, when $\phi_A = \phi_B + \pi$.

Finally, consider the case shown in Fig. 5(c) where all three segments are topological. Here the Majoranas $\gamma_{1,2,3}$ couple

via

$$H_{123} \propto -i\Gamma \left[\cos\left(\frac{\phi_A - \phi_B}{2}\right) \gamma_1 \gamma_2 + \cos\left(\frac{\phi_C - \phi_B}{2}\right) \gamma_3 \gamma_2 + \sin\left(\frac{\phi_A - \phi_C}{2}\right) \gamma_1 \gamma_3 \right]. \quad (11)$$

Note the sine function determining the coupling between γ_1 and γ_3 , which arises because of the conventions we chose for defining ϕ_α above. Recall that to make the problem well-defined, we needed to define the phases with respect to a particular direction in each wire; otherwise there is an ambiguity of π in the definition, since for instance $|\Delta|e^{i\phi}c_jc_{j+1} = |\Delta|e^{i(\phi+\pi)}c_{j+1}c_j$. We defined the phases such that the site indices increase upon moving rightward or upward in the wires. But this implies that the site indices in both the left and bottom wires increase upon moving towards the junction, in contrast to all other pairs of wires. It follows that the splitting of γ_1 and γ_3 is proportional to $\cos[(\phi_A - \phi_C - \pi)/2] = \sin[(\phi_A - \phi_C)/2]$. Hence with our conventions a π junction between these two regions actually corresponds to the case $\phi_A = \phi_C$.

The Hamiltonian H_{123} implies that $\gamma_{1,2,3}$ all remain zero-energy modes only when $\phi_A = \phi_C = \phi_B + \pi$, where all pairs of wires form mutual π junctions. (This remains true even when coupling to the ordinary gapped states is included.) Aside from this fine-tuned limit, however, H_{123} always supports one zero-energy Majorana mode and one ordinary finite-energy fermion. As an illustration, consider the case $\phi_A = \phi_B + \pi$ and $\phi_C \neq \phi_A$, so that only the horizontal wires form a π junction. Here the Hamiltonian simplifies to

$$H_{123} \propto -i\Gamma \cos\left(\frac{\phi_C - \phi_B}{2}\right) \gamma_3(\gamma_2 - \gamma_1). \quad (12)$$

It follows that the linear combination $(\gamma_1 + \gamma_2)/\sqrt{2}$ remains a zero-energy Majorana mode, while γ_3 and $(\gamma_1 - \gamma_2)/\sqrt{2}$ fuse to a finite-energy state. While here the zero-energy Majorana carries weight only on the horizontal wires which formed the π junction, in general its wavefunction will have weight on all three segments.

As we braid Majorana fermions using the methods described in the main text, it is imperative that we avoid generating spurious zero-modes at the T-junction. The above discussion implies that we are safe in this regard so long as we avoid π junctions. Fortunately, the semiconducting wires we considered naturally avoid such situations, since two wires at right angles to one another exhibit effective p -wave phases that differ by $\pi/2$ as discussed in the main text.

B. Wavefunction approach to Majorana fermion exchange

In this section we provide alternative derivations (and additional details) for the transformation rule obtained in the main text for exchange of two Majorana fermions. First, we will consider the process outlined in Figs. 3(a)-(d) and study the

exchange from the perspective of the ground state wavefunctions. Second, we will consider a simple exactly solvable four-site problem that allows us to similarly analyze an exchange of the type sketched in Figs. 3(e)-(h). We will demonstrate that the transformation rule here is identical to the topologically equivalent braid in Figs. 3(a)-(d) as claimed in the main text.

1. Exchange in a system with two Majorana fermions

Consider now the initial setup in Fig. 3(a). As in the main text we will assume that each wire in the T-junction is described by Kitaev's toy lattice model. For concreteness let us assume that the horizontal wire consists of $2N + 1$ sites while the vertical wire consists of N sites as Fig. 6 illustrates. Additionally, let c_x and \tilde{c}_y respectively denote the spinless fermion operators in the horizontal and vertical chains. In the initial configuration the vertical wire is non-topological, while the horizontal wire is topological and thus exhibits end Majorana fermions which we would like to exchange. We will follow the strategy adopted in the main text and keep the Hamiltonian purely real during this exchange (until the very end, when we will allow the Hamiltonian to become complex). Again, this assumption has the virtue that the wavefunctions can then also be chosen real, so that in spite of their complex evolution the Berry phase accumulated as the Majoranas are transported vanishes identically.

For convenience we will further deform the Hamiltonian describing this initial setup to the following:

$$H_i = -\tilde{\mu} \sum_{y=1}^N \tilde{c}_y^\dagger \tilde{c}_y + t \sum_{x=1}^{2N} (c_x^\dagger + c_x)(c_{x+1}^\dagger - c_{x+1}), \quad (13)$$

with $\tilde{\mu} < 0$ and $t > 0$. The first term implies that all \tilde{c}_y fermions in the vertical wire will be absent in the initial ground state, while the second can be recognized as Kitaev's toy model in the special limit where $\mu = 0$, $t = |\Delta|$, and the superconducting phase is $\phi = 0$. We graphically denote this initial superconducting phase by the rightward-pointing arrow in Fig 3(a) (a leftward-pointing arrow would indicate a phase of π , which would also keep the Hamiltonian purely real). The end Majorana fermions for the horizontal wire take on a particularly simple form, allowing the initial wavefunctions to be easily obtained.

As shown by Kitaev¹⁸ and outlined in the main text, decomposing c_x in terms of Majorana fermions $\gamma_{A/B,x}$ via

$$c_x = \frac{1}{2}(\gamma_{B,x} + i\gamma_{A,x}) \quad (14)$$

allows the Hamiltonian to be written as

$$H_i = -\tilde{\mu} \sum_{y=1}^N \tilde{c}_y^\dagger \tilde{c}_y - it \sum_{x=1}^{2N} \gamma_{B,x} \gamma_{A,x+1}. \quad (15)$$

The zero-energy end Majorana fermions $\gamma_{A,1}$ and $\gamma_{B,2N+1}$ which do not appear in H can be combined into an ordinary

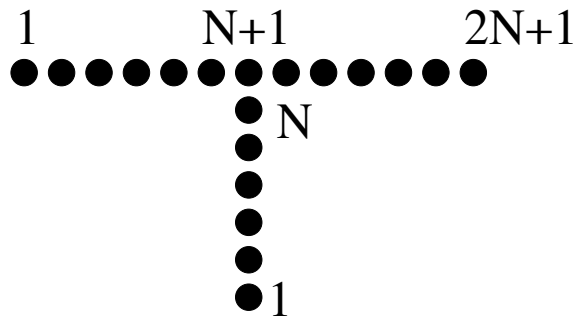


FIG. 6: Lattice structure giving rise to the T-junction.

zero-energy fermion

$$d_{\text{end}} = \frac{1}{2}(\gamma_{A,1} + i\gamma_{B,2N+1}), \quad (16)$$

while the gapped bulk states are captured by operators

$$d_x = \frac{1}{2}(\gamma_{A,x+1} + i\gamma_{B,x}). \quad (17)$$

In terms of d_x , H_i becomes

$$H_i = -\tilde{\mu} \sum_{y=1}^N \tilde{c}_y^\dagger \tilde{c}_y + t \sum_{x=1}^{2N} (2d_x^\dagger d_x - 1). \quad (18)$$

The Majorana end states give rise to two degenerate initial ground states whose evolution we are interested in: $|0\rangle_i$ which is annihilated by d_{end} and $|1\rangle_i = d_{\text{end}}^\dagger |0\rangle_i$. The former can be written $|0\rangle_i = \prod_{x=1}^{2N} d_x |\text{vac}\rangle$, where $|\text{vac}\rangle$ denotes the vacuum of c_x and \tilde{c}_y fermions (d_{end} indeed annihilates $|0\rangle_i$ as defined here). After some algebra, the normalized ground states can be written explicitly as

$$\begin{aligned} |0\rangle_i &= \frac{1}{2^N} \left[1 + \sum_{p=1}^N \sum_{i_1 < \dots < i_{2p}}^{2N+1} c_{i_{2p}}^\dagger \dots c_{i_1}^\dagger \right] |\text{vac}\rangle \\ |1\rangle_i &= \frac{1}{2^N} \sum_{p=0}^N \sum_{i_1 < \dots < i_{2p+1}}^{2N+1} c_{i_{2p+1}}^\dagger \dots c_{i_1}^\dagger |\text{vac}\rangle. \end{aligned} \quad (19)$$

Note that we have multiplied $|0\rangle_i$ and $|1\rangle_i$ by overall phase factors to make each wavefunction purely real. Although the ground states have different fermion parity, both yield the same average particle number

$$\bar{N} = \frac{2N+1}{2} \quad (20)$$

corresponding to half-filling of the horizontal chain.

Let us now transport the Majorana fermions as outlined in Figs. 3(a)-(d), keeping the Hamiltonian (and ground state wavefunctions) real and avoiding generating additional zero-energy modes. For example, γ_1 can be transported rightward one site by adding the following term to H_i ,

$$\delta H = -\lambda \mu c_1^\dagger c_1 - \lambda t (c_1^\dagger + c_1)(c_2^\dagger - c_2) \quad (21)$$

(with $\mu < 0$) and varying λ from 0 to 1. As emphasized in the main text, a subtle but essential point is that as we so transport γ_1 and γ_2 we must avoid having two neighboring topological regions whose superconducting phases differ by π , for in this case a pair of ‘accidental’ zero-energy Majorana modes appears at the junction. It is therefore useful to employ arrows as shown in Figs. 3(a)-(d) to signify the sign of the pairing in each topological region. Two inward or two outward arrows meeting at the junction correspond to a π junction and must be avoided. Figures 3(a)-(d) illustrate that in accordance with this simple rule, we can indeed swap the positions of γ_1 and γ_2 while keeping the Hamiltonian and wavefunctions purely real, consequently acquiring no Berry phase in the process. However, the arrows and hence the sign of the pairing in the topological region unavoidably reverse, as seen by comparing Figs. 3(a) and (d). Thus we have not yet completed an exchange in the usual sense.

At this stage we have adiabatically evolved the Hamiltonian to

$$H' = -\tilde{\mu} \sum_{y=1}^N \tilde{c}_y^\dagger \tilde{c}_y - t \sum_{x=1}^{2N} (c_x^\dagger - c_x)(c_{x+1}^\dagger + c_{x+1}), \quad (22)$$

corresponding to H_i with the sign of the pairing reversed, and the wavefunctions to

$$\begin{aligned} |0\rangle' &= \frac{1}{2^N} \left[1 + \sum_{p=1}^N \sum_{i_1 < \dots < i_{2p}}^{2N+1} (-1)^p c_{i_{2p}}^\dagger \dots c_{i_1}^\dagger \right] |\text{vac}\rangle \\ |1\rangle' &= \frac{1}{2^N} \sum_{p=0}^N \sum_{i_1 < \dots < i_{2p+1}}^{2N+1} (-1)^p c_{i_{2p+1}}^\dagger \dots c_{i_1}^\dagger |\text{vac}\rangle. \quad (23) \end{aligned}$$

[Modulo phase factors, these wavefunctions can be obtained by sending $c_x \rightarrow ic_x$ in Eqs. (19).] To complete the exchange, let us now return the Hamiltonian to its original form by adiabatically rotating the superconducting phase in the topological region from π back to 0. The Hamiltonian then involves complex matrix elements, which implies that Berry phases need no longer vanish here. As we will see, however, the Berry phase contributions for this final step can be easily calculated.

To this end, consider

$$\begin{aligned} H(\lambda) &= -\tilde{\mu} \sum_{y=1}^N \tilde{c}_y^\dagger \tilde{c}_y - t \sum_{x=1}^{2N} (e^{i\lambda\pi/2} c_x^\dagger - e^{-i\lambda\pi/2} c_x) \\ &\times (e^{i\lambda\pi/2} c_{x+1}^\dagger + e^{-i\lambda\pi/2} c_{x+1}). \quad (24) \end{aligned}$$

Upon varying λ from 0 to 1, the superconducting phase rotates by π such that $H(\lambda = 0) = H'$ and $H(\lambda = 1) = H_i$ as

desired. The ground states of $H(\lambda)$ are

$$\begin{aligned} |0(\lambda)\rangle &= \frac{e^{i\lambda\theta}}{2^N} \left[1 + \sum_{p=1}^N \sum_{i_1 < \dots < i_{2p}}^{2N+1} (-1)^p e^{i\lambda\pi p} \right. \\ &\times \left. c_{i_{2p}}^\dagger \dots c_{i_1}^\dagger \right] |\text{vac}\rangle \\ |1(\lambda)\rangle &= \frac{e^{i\lambda\theta}}{2^N} \sum_{p=0}^N \sum_{i_1 < \dots < i_{2p+1}}^{2N+1} (-1)^p e^{i\lambda\pi(p+1/2)} \\ &\times c_{i_{2p+1}}^\dagger \dots c_{i_1}^\dagger |\text{vac}\rangle. \quad (25) \end{aligned}$$

Importantly, $|0(\lambda = 0)\rangle = |0\rangle'$ and $|1(\lambda = 0)\rangle = |1\rangle'$ so that the wavefunctions evolve smoothly throughout. Note also that we have inserted an arbitrary phase factor θ above. We will select this phase momentarily such that the Berry phase acquired by each wavefunction during this final stage also vanishes. The outcome of the exchange is then simpler to interpret, since one simply compares the initial states $|0\rangle_i$ and $|1\rangle_i$ with the final states $|0\rangle_f \equiv |0(\lambda = 1)\rangle$ and $|1\rangle_f \equiv |1(\lambda = 1)\rangle$.

Using Eqs. (25), one can now compute the Berry phases; we find

$$\begin{aligned} \text{Im} \int_0^1 d\lambda \langle 0(\lambda) | \partial_\lambda | 0(\lambda) \rangle &= \text{Im} \int_0^1 d\lambda \langle 1(\lambda) | \partial_\lambda | 1(\lambda) \rangle \\ &= \theta + \frac{\bar{N}\pi}{2}. \quad (26) \end{aligned}$$

(Off-diagonal components such as $\langle 0(\lambda) | \partial_\lambda | 1(\lambda) \rangle$ vanish trivially due to the different fermion parity of the ground states.) This result is quite sensible given that both wavefunctions describe on average $\bar{N}/2$ Cooper pairs whose phase rotates by π . We now choose

$$\theta = -\frac{\bar{N}\pi}{2} \quad (27)$$

so that the Berry phases vanish as desired. Only the explicit relative phases between the initial and final wavefunctions remain. For $\lambda = 1$ the factors of $(-1)^p$ cancel in Eqs. (25), yielding

$$\begin{aligned} |0\rangle_f &= e^{-i\bar{N}\pi/2} |0\rangle_i \\ |1\rangle_f &= i e^{-i\bar{N}\pi/2} |1\rangle_i. \quad (28) \end{aligned}$$

Crucially, the ground state $|1\rangle$ acquires an additional phase factor of i relative to $|0\rangle$ under the exchange. Neglecting an overall phase factor, the unitary operator that generates this relative phase can be written

$$U_{12} = e^{i\frac{\pi}{4}(2d_{\text{end}}^\dagger d_{\text{end}} - 1)} = e^{i\frac{\pi}{4}\gamma_2\gamma_1}, \quad (29)$$

where we have identified $\gamma_1 = \gamma_{A,1}$ and $\gamma_2 = \gamma_{B,2N+1}$. This coincides with the expression obtained in the main text by somewhat different means, and is identical to the unitary operator generating the exchange of vortices in a spinless $p + ip$ superconductor⁷.

As an aside, we comment that we have chosen in Eq. (24) to rotate the superconducting phase clockwise from π to 0 in

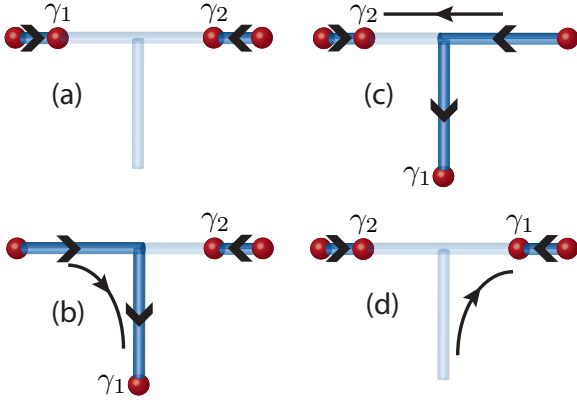


FIG. 7: Exchange of two Majorana fermions separated by a non-topological region. Here we envision transporting the Majoranas while keeping the Hamiltonian purely real. The superconducting phase in the topological regions can then only take on two values, 0 or π , which we indicate by arrows above. Unlike in the exchange of Figs. 3(a)-(d), here we can exchange Majorana fermions while keeping the Hamiltonian purely real, maintaining the gap, and returning the Hamiltonian back to its original form (*i.e.*, without reversing the sign of the pairing). As explained in the text, this does *not* mean that the exchange is trivial; indeed, the Majoranas transform exactly as they do in the topologically equivalent braid of Figs. 3(a)-(d).

the final step of the exchange. Had we alternatively chosen to rotate the phase in a counterclockwise fashion, the ground state $|1\rangle$ would pick up a relative phase of $-i$ under the exchange compared to $|0\rangle$. We stress that this does not at all affect the conclusion of non-Abelian statistics. A similar ambiguity arises in Ivanov’s construction⁷, since the relative sign that arises in the $p + ip$ context depends on whether one takes the branch cuts emanating ‘upwards’ or ‘downwards’ from the vortices.

2. Exchange in a toy model exhibiting four Majorana modes

We next examine by similar means an exchange of the type outlined in Figs. 3(e)-(h). This braid is topologically equivalent to the one considered above and displayed in Figs. 3(a)-(d), so the Majoranas must transform in an identical manner under exchange. Demonstrating this equivalence, however, is rather nontrivial. Suppose we proceed as we did earlier for the exchange of Figs. 3(a)-(d) and transport $\gamma_{1,2}$ while keeping the Hamiltonian purely real to avoid Berry phase accumulation. It is once again instructive to view the sign of the pairing in the topological regions with arrows as displayed in Figs. 7(a)-(d). As the figure illustrates, it is now possible to exchange γ_1 and γ_2 *without* reversing the sign of the pairing in the process. In other words, we can keep the Hamiltonian purely real, swap the locations of the Majoranas, and return the Hamiltonian back to its original form—without closing a gap. One may worry, then, that this type of exchange is trivial, but this is not so.

The subtlety arises because there are now four Majorana fermions rather than two, and in this case one gets less mileage

out of keeping the Hamiltonian real during the exchange. To illustrate the point, let $\gamma_{1,2}$ denote the Majoranas we wish to exchange, and $\gamma_{3,4}$ the stationary Majoranas of Figs. 3(e)-(h). Defining

$$\begin{aligned} f_A &= \frac{1}{2}(\gamma_1 + i\gamma_2) \\ f_B &= \frac{1}{2}(\gamma_3 + i\gamma_4), \end{aligned} \quad (30)$$

we see that there are now two degenerate ground states in each fermion parity sector: $|0, 0\rangle$ which both f_A and f_B annihilate, $|1, 1\rangle = f_A^\dagger f_B^\dagger |0, 0\rangle$, $|1, 0\rangle = f_A^\dagger |0, 0\rangle$, and $|0, 1\rangle = f_B^\dagger |0, 0\rangle$. Reality of the Hamiltonian does *not* imply that these four ground states can each be chosen real. Indeed, we provide an example below where this is clearly not possible. Rather, this condition only guarantees reality of specific linear combinations of these ground states, which in general can vary as the exchange takes place. In other words, the reality condition does not preclude the phases of the above ground states from evolving nontrivially during the exchange (see below for an explicit example). Drawing conclusions about the exchange from this route therefore requires a more detailed analysis than in the case with only two Majorana fermions. To remedy this issue, one might be tempted to modify the setup of Figs. 3(e)-(h) by connecting the horizontal wire into a loop, then fusing γ_3 and γ_4 so that only the two Majoranas which we exchange remain. One will quickly discover, however, that in this case the positions of γ_1 and γ_2 can not be swapped while keeping the Hamiltonian real and all other excitations gapped. Specifically, in the process one necessarily ends up with a configuration similar to Fig. 7(c), except with two arrows pointing either into or out of the junction; that is, one can not avoid π junctions here.

We will therefore proceed by considering a toy problem that provides an illustrative minimal setting in which such an exchange can be analyzed explicitly. Specifically, we examine the four-site setup shown in Fig. 8 and described by the following purely real Hamiltonian:

$$\begin{aligned} H &= -\mu c_4^\dagger c_4 + t(c_1^\dagger + c_1)[(c_2^\dagger - c_2) + (c_3^\dagger - c_3)] \\ &\quad + [t_{24}(c_2^\dagger + c_2) + t_{34}(c_3^\dagger + c_3)](c_4^\dagger - c_4), \end{aligned} \quad (31)$$

with $t > 0$, $\mu \leq 0$, and $t_{24}, t_{34} \geq 0$. In spite of the small number of sites, this Hamiltonian supports four zero-energy Majorana modes for any values of μ , t_{24} , and t_{34} . To get intuition here, it is useful to think of site 1 as forming a π junction between sites 2 and 3. This gives rise to two Majorana modes which are independent of the parameters appearing in Eq. (31). One of these, γ_3 , resides at site 1:

$$\gamma_3 = i(c_1^\dagger - c_1). \quad (32)$$

The other, γ_4 , resides on sites 2 and 3:

$$\gamma_4 = \frac{i}{\sqrt{2}}(c_2^\dagger - c_2 - c_3^\dagger + c_3). \quad (33)$$

The locations of the second pair of Majoranas, γ_1 and γ_2 , depend on μ , t_{24} , and t_{34} . We will vary these parameters so

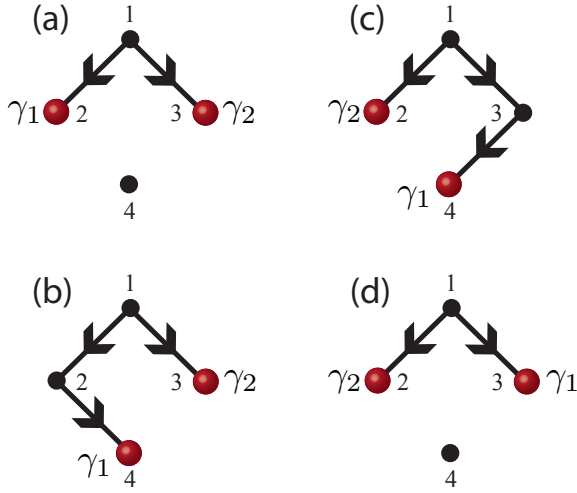


FIG. 8: Minimal four-site setup that supports four Majorana modes (only γ_1 and γ_2 are shown for clarity). The Hamiltonian is chosen so as to exchange γ_1 and γ_2 as sketched in (a)-(d), mimicking the exchange of Fig. 3(e)-(h) in a tractable setup. Solid lines denote bonds with non-zero pairing whose sign is indicated by the arrows.

as to carry out an exchange of γ_1 and γ_2 in a manner that is analogous to the exchange of Figs. 3(e)-(h).

To help establish a connection between the setup of Fig. 3(e) and the present four site-problem, imagine first forming a loop out of the horizontal wire so that the two topological regions connect. The outer Majoranas of Fig. 3(e)—which are analogous to $\gamma_{3,4}$ in our setup—can then be generated by forming a π junction in the topological region. The four-site problem shrinks this π junction to the smallest possible size. The other two Majoranas $\gamma_{1,2}$ will initially be separated by an unpaired region, similar to the non-topological segments connecting $\gamma_{1,2}$ in Fig. 3(e). We carry out their exchange piecewise in three stages to reduce the algebraic complexity of the problem. Care will be taken to ensure that the wavefunctions and operators defined below evolve continuously in between each of these stages.

(I) In the first stage, we evolve the Hamiltonian by taking

$$\begin{aligned}\mu &= (1 - \lambda)\mu_4 \\ t_{24} &= \lambda t \\ t_{34} &= 0\end{aligned}\quad (34)$$

(with $\mu_4 < 0$) and varying λ from 0 to 1. Initially when $\lambda = 0$, γ_1 and γ_2 are situated at sites 2 and 3, respectively, as Fig. 8(a) illustrates. Ramping up λ to 1 shuttles γ_1 to site 4, leading to the configuration of Fig. 8(b). More precisely, $\gamma_{1,2}$ are given by

$$\gamma_1^I = \frac{1}{\alpha_{24}}[-\mu(c_2^\dagger + c_2) + 2t_{24}(c_4^\dagger + c_4)] \quad (35)$$

$$\gamma_2^I = c_3^\dagger + c_3, \quad (36)$$

where we have defined $\alpha_{24} = \sqrt{4t_{24}^2 + \mu^2}$. The finite-energy

fermion operators which annihilate the ground states are

$$\begin{aligned}d_A^I &= \frac{1}{2\sqrt{2}}[\sqrt{2}(c_1^\dagger + c_1) + (c_2^\dagger - c_2) + (c_3^\dagger - c_3)] \quad (37) \\ d_B^I &= \frac{1}{2\alpha_{24}}[2t_{24}(c_2^\dagger + c_2) + (\mu + \alpha_{24})c_4^\dagger + (\mu - \alpha_{24})c_4].\end{aligned}\quad (38)$$

Now define f_A^I and f_B analogously to Eqs. (30). Suppressing the λ dependence for notational simplicity, the four degenerate ground states are then

$$\begin{aligned}|0, 0\rangle_I \\ |1, 1\rangle_I &= f_A^{I\dagger} f_B^\dagger |0, 0\rangle_I \\ |1, 0\rangle_I &= f_A^{I\dagger} |0, 0\rangle_I \\ |0, 1\rangle_I &= f_B^\dagger |0, 0\rangle_I,\end{aligned}\quad (39)$$

where $|0, 0\rangle_I$ is annihilated by f_A^I, f_B, d_A^I , and d_B^I . With the above definitions and some time to carry out the algebra, one can obtain these ground states for arbitrary λ . When $\lambda = 0$ leading to the initial configuration shown in Fig. 8(a), the wavefunctions are

$$\begin{aligned}|0, 0\rangle_i &= \frac{1}{2}[-i - e^{i\frac{\pi}{4}}c_2^\dagger c_1^\dagger + e^{-i\frac{\pi}{4}}c_3^\dagger c_1^\dagger + c_3^\dagger c_2^\dagger]|\text{vac}\rangle \\ |1, 1\rangle_i &= \frac{1}{2}[e^{-i\frac{\pi}{4}} + c_2^\dagger c_1^\dagger - ic_3^\dagger c_1^\dagger - e^{i\frac{\pi}{4}}c_3^\dagger c_2^\dagger]|\text{vac}\rangle \quad (40) \\ |1, 0\rangle_i &= \frac{1}{2}[-e^{i\frac{\pi}{4}}c_1^\dagger - ic_2^\dagger - c_3^\dagger - e^{-i\frac{\pi}{4}}c_3^\dagger c_2^\dagger c_1^\dagger]|\text{vac}\rangle \\ |0, 1\rangle_i &= \frac{1}{2}[c_1^\dagger + e^{-i\frac{\pi}{4}}c_2^\dagger + e^{i\frac{\pi}{4}}c_3^\dagger + ic_3^\dagger c_2^\dagger c_1^\dagger]|\text{vac}\rangle.\end{aligned}$$

Clearly none of these can be made real by introducing overall phase factors (though one can readily verify that a purely real basis does exist by considering linear combinations of these states). When $\lambda \rightarrow 1$ and we arrive at the configuration shown in Fig. 8(b), the wavefunctions evolve to

$$\begin{aligned}|0, 0\rangle_b &= \frac{1}{2\sqrt{2}}[-i - e^{i\frac{\pi}{4}}c_2^\dagger c_1^\dagger + e^{-i\frac{\pi}{4}}c_3^\dagger c_1^\dagger - e^{i\frac{\pi}{4}}c_4^\dagger c_1^\dagger \\ &\quad + c_3^\dagger c_2^\dagger - ic_4^\dagger c_2^\dagger - c_4^\dagger c_3^\dagger - e^{-i\frac{\pi}{4}}c_4^\dagger c_3^\dagger c_2^\dagger c_1^\dagger]|\text{vac}\rangle \\ |1, 1\rangle_b &= \frac{1}{2\sqrt{2}}[e^{-i\frac{\pi}{4}} + c_2^\dagger c_1^\dagger - ic_3^\dagger c_1^\dagger + c_4^\dagger c_1^\dagger - e^{i\frac{\pi}{4}}c_3^\dagger c_2^\dagger \\ &\quad + e^{-i\frac{\pi}{4}}c_4^\dagger c_2^\dagger + e^{i\frac{\pi}{4}}c_4^\dagger c_3^\dagger + ic_4^\dagger c_3^\dagger c_2^\dagger c_1^\dagger]|\text{vac}\rangle \quad (41) \\ |1, 0\rangle_b &= \frac{1}{2\sqrt{2}}[-e^{i\frac{\pi}{4}}c_1^\dagger - ic_2^\dagger - c_3^\dagger - ic_4^\dagger - e^{-i\frac{\pi}{4}}c_3^\dagger c_2^\dagger c_1^\dagger \\ &\quad - e^{i\frac{\pi}{4}}c_4^\dagger c_2^\dagger c_1^\dagger + e^{-i\frac{\pi}{4}}c_4^\dagger c_3^\dagger c_1^\dagger + c_4^\dagger c_3^\dagger c_2^\dagger]|\text{vac}\rangle \\ |0, 1\rangle_b &= \frac{1}{2\sqrt{2}}[c_1^\dagger + e^{-i\frac{\pi}{4}}c_2^\dagger + e^{i\frac{\pi}{4}}c_3^\dagger + e^{-i\frac{\pi}{4}}c_4^\dagger \\ &\quad + ic_3^\dagger c_2^\dagger c_1^\dagger + c_4^\dagger c_2^\dagger c_1^\dagger - ic_4^\dagger c_3^\dagger c_1^\dagger - e^{i\frac{\pi}{4}}c_4^\dagger c_3^\dagger c_2^\dagger]|\text{vac}\rangle.\end{aligned}$$

(II) For the second stage of the exchange, we evolve the Hamiltonian according to

$$\begin{aligned}\mu &= 0 \\ t_{24} &= (1 - \lambda)t \\ t_{34} &= \lambda t.\end{aligned}\quad (42)$$

Here varying λ from 0 to 1 leaves γ_1 unchanged but adiabatically transports γ_2 from site 3 to site 2, leading to the configuration of Fig. 8(c). Defining $\beta = \sqrt{t_{34}^2 + t_{24}^2}$, the Majorana fermion operators at this stage obey

$$\gamma_1^{II} = c_4^\dagger + c_4 \quad (43)$$

$$\gamma_2^{II} = \frac{1}{\beta}[-t_{34}(c_2^\dagger + c_2) + t_{24}(c_3^\dagger + c_3)], \quad (44)$$

while the gapped quasiparticle operators are

$$d_A^{II} = d_A^I \quad (45)$$

$$d_B^{II} = \frac{1}{2\beta}[t_{24}(c_2^\dagger + c_2) + t_{34}(c_3^\dagger + c_3) + \beta(c_4^\dagger - c_4)] \quad (46)$$

The wavefunctions can again be obtained for arbitrary λ after some tedious algebra. In particular, when $\lambda \rightarrow 1$ bringing the system to the setup of Fig. 8(c), the wavefunctions evolve to

$$\begin{aligned} |0,0\rangle_c &= \frac{1}{2\sqrt{2}}[-i - e^{i\frac{\pi}{4}}c_2^\dagger c_1^\dagger + e^{-i\frac{\pi}{4}}c_3^\dagger c_1^\dagger + e^{-i\frac{\pi}{4}}c_4^\dagger c_1^\dagger \\ &\quad + c_3^\dagger c_2^\dagger + c_4^\dagger c_2^\dagger - ic_4^\dagger c_3^\dagger - e^{i\frac{\pi}{4}}c_4^\dagger c_3^\dagger c_2^\dagger c_1^\dagger]|\text{vac}\rangle \\ |1,1\rangle_c &= \frac{1}{2\sqrt{2}}[e^{i\frac{\pi}{4}} + ic_2^\dagger c_1^\dagger + c_3^\dagger c_1^\dagger + c_4^\dagger c_1^\dagger + e^{-i\frac{\pi}{4}}c_3^\dagger c_2^\dagger \\ &\quad + e^{-i\frac{\pi}{4}}c_4^\dagger c_2^\dagger + e^{i\frac{\pi}{4}}c_4^\dagger c_3^\dagger + ic_4^\dagger c_3^\dagger c_2^\dagger c_1^\dagger]|\text{vac}\rangle \quad (47) \\ |1,0\rangle_c &= \frac{1}{2\sqrt{2}}[e^{-i\frac{\pi}{4}}c_1^\dagger + c_2^\dagger - ic_3^\dagger - ic_4^\dagger - e^{i\frac{\pi}{4}}c_3^\dagger c_2^\dagger c_1^\dagger \\ &\quad - e^{i\frac{\pi}{4}}c_4^\dagger c_2^\dagger c_1^\dagger + e^{-i\frac{\pi}{4}}c_4^\dagger c_3^\dagger c_1^\dagger + c_4^\dagger c_3^\dagger c_2^\dagger]|\text{vac}\rangle \\ |0,1\rangle_c &= \frac{1}{2\sqrt{2}}[c_1^\dagger + e^{-i\frac{\pi}{4}}c_2^\dagger + e^{i\frac{\pi}{4}}c_3^\dagger + e^{i\frac{\pi}{4}}c_4^\dagger \\ &\quad + ic_3^\dagger c_2^\dagger c_1^\dagger + ic_4^\dagger c_2^\dagger c_1^\dagger + c_4^\dagger c_3^\dagger c_1^\dagger + e^{-i\frac{\pi}{4}}c_4^\dagger c_3^\dagger c_2^\dagger]|\text{vac}\rangle. \end{aligned}$$

Notice how the phase factors in the wavefunctions evolve non-trivially in passing from Eqs. (41) to (47), despite the reality of the Hamiltonian.

(III) To conclude the exchange, we now choose

$$\begin{aligned} \mu &= \lambda\mu_4 \\ t_{24} &= 0 \\ t_{34} &= (1 - \lambda)t \end{aligned} \quad (48)$$

and again vary λ from 0 to 1. In this final step, γ_2 remains unchanged while γ_1 moves adiabatically to site 3 as in Fig. 8(d). The Majorana operators now obey

$$\gamma_1^{III} = \frac{1}{\alpha_{34}}[-\mu(c_3^\dagger + c_3) + 2t_{34}(c_4^\dagger + c_4)] \quad (49)$$

$$\gamma_2^{III} = -(c_2^\dagger + c_2), \quad (50)$$

with $\alpha_{34} = \sqrt{4t_{34}^2 + \mu^2}$, and the gapped quasiparticle operators are

$$d_A^{III} = d_A^I \quad (51)$$

$$d_B^{III} = \frac{1}{2\alpha_{34}}[2t_{34}(c_3^\dagger + c_3) + (\mu + \alpha_{34})c_4^\dagger + (\mu - \alpha_{34})c_4]. \quad (52)$$

Computing the ground states as before, we obtain the remarkable result that the final and initial ground states are related by

$$\begin{aligned} |0,0\rangle_f &= |0,0\rangle_i \\ |1,1\rangle_f &= i|1,1\rangle_i \\ |1,0\rangle_f &= i|1,0\rangle_i \\ |0,1\rangle_f &= |0,1\rangle_i. \end{aligned} \quad (53)$$

That is, the ground states with an $f_A = (\gamma_1 + i\gamma_2)/2$ fermion present acquire a phase factor of i under the exchange. Up to an overall unimportant phase factor, this transformation is generated by the unitary operator $U_{12} = e^{\pi\gamma_2\gamma_1/4}$, which is precisely what we obtained earlier under quite different circumstances. This should not be surprising, however, since again this reflects a topological result that must have worked out in this way.

To close this section, we remark that one may object that in obtaining this result we have simply compared the initial and final states. Since the above wavefunctions are not real, one may in particular ask whether the exchange is tainted by Berry phases. It is not—it is always possible to simply change to a real basis by suitably superposing these wavefunctions, and in such a basis the absence of Berry phases is manifest. The exchange indeed is governed solely by the difference between initial and final states.

C. Derivation of the fractional Josephson effect in a simple model

For pedagogical purposes, we will review here the ‘fractional Josephson effect’ originally predicted by Kitaev¹⁸ and discussed by other authors in the context of one-dimensional wires^{1,2} and other topological systems^{10,20,29,30}. We will examine this effect in a minimal setup where all calculations can be explicitly carried out, although the qualitative aspects of the physics are more universal. Consider two topological superconducting wires forming a Josephson junction as shown schematically in Fig. 9(a). The phases of the p -wave order parameters are taken to be $\phi_{L/R}$ in the left/right wires, which are coupled by a weak (compared to the gap in each wire) electron tunneling term at the junction. The full Hamiltonian reads

$$H = H_L + H_R + H_\Gamma, \quad (54)$$

where $H_{L/R}$ describe the left/right regions and H_Γ represents the electron tunneling term coupling the wires. For computational simplicity, we model the left and right regions as N -site chains described by Kitaev’s toy model with $\mu = 0$ and $t = |\Delta|$. In this case we have

$$\begin{aligned} H_\alpha &= t \sum_{x=1}^{N-1} (e^{-i\phi_\alpha/2} c_{\alpha,x}^\dagger + e^{i\phi_\alpha/2} c_{\alpha,x}) \\ &\quad \times (e^{-i\phi_\alpha/2} c_{\alpha,x+1}^\dagger - e^{i\phi_\alpha/2} c_{\alpha,x+1}), \end{aligned} \quad (55)$$

for $\alpha = L/R$, along with a tunneling term

$$H_\Gamma = -\Gamma(c_{L,N}^\dagger c_{R,1} + h.c.). \quad (56)$$

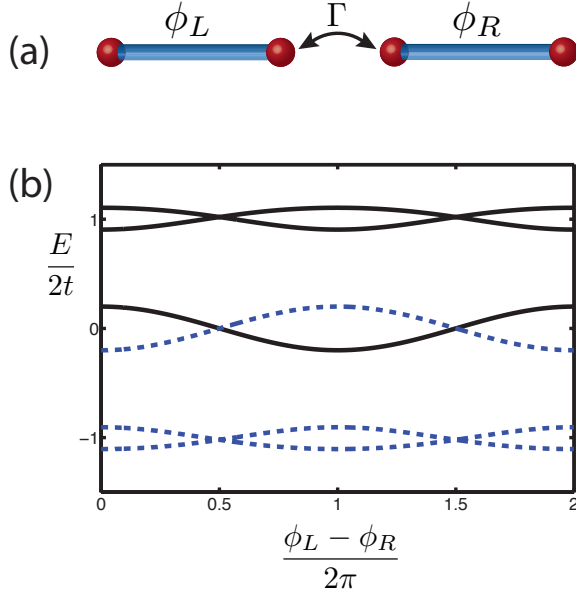


FIG. 9: (a) Schematic of the Josephson junction formed by two topological wires with p -wave superconducting phases $\phi_{L/R}$. The wires couple at the junction through an electron tunneling term with strength Γ . (b) Bogoliubov-de Gennes spectrum as a function of $(\phi_L - \phi_R)/(2\pi)$ for the effective Hamiltonian in Eq. (65) chosen to describe the junction. Only the solid lines denote physically distinct states. The states centered around $E/(2t) = 1$ represent ordinary bulk quasiparticles, while the state near zero energy represents the quasiparticle formed when the two end Majoranas at the junction fuse. The energy and hence Josephson current corresponding to the latter exhibit 4π periodicity in $\phi_L - \phi_R$. The ordinary bulk quasiparticle states, however, contribute only to the usual 2π -periodic Josephson effect.

When $\Gamma = 0$, two Majorana fermions reside at the junction; turning on $\Gamma \neq 0$ generally fuses these to an ordinary finite-energy quasiparticle state. We wish to compute the zero-bias current flowing across the junction,

$$I = -\frac{e\Gamma}{\hbar} \langle i c_{L,N}^\dagger c_{R,1} + h.c. \rangle, \quad (57)$$

in the ground state as well as the excited state where this quasiparticle state is occupied.

We proceed by first diagonalizing $H_{L/R}$ in the usual way. Writing $c_{\alpha,x} = e^{-i\phi_\alpha/2}(\gamma_{B,\alpha}^\dagger + i\gamma_{A,\alpha})/2$ and then defining $d_{\alpha,x} = (\gamma_{A,\alpha}^\dagger + i\gamma_{B,\alpha})/2$, one obtains

$$H_\alpha = t \sum_{x=1}^{N-1} (2d_{\alpha,x}^\dagger d_{\alpha,x} - 1). \quad (58)$$

It is useful to group the end Majorana fermions residing at the junction into an ordinary fermion operator via

$$d_{\text{end}} = \frac{1}{2}(\gamma_{A,1}^R + i\gamma_{B,N}^L). \quad (59)$$

The tunneling term, which we will treat as a perturbation, can

then be written

$$\begin{aligned} H_\Gamma &= \frac{\Gamma}{2} \{ C [d_{R,1}^\dagger (d_{L,N-1}^\dagger + d_{L,N-1}) + h.c.] \\ &\quad + S [i d_{\text{end}}^\dagger (d_{R,1}^\dagger - d_{R,1} + d_{L,N-1}^\dagger + d_{L,N-1}) + h.c.] \\ &\quad + C (2d_{\text{end}}^\dagger d_{\text{end}} - 1) \} \end{aligned} \quad (60)$$

with

$$C = \cos(\Delta\phi/2) \quad (61)$$

$$S = \sin(\Delta\phi/2) \quad (62)$$

$$\Delta\phi = \phi_L - \phi_R. \quad (63)$$

Rewriting the expression for the current in this basis, one obtains the familiar relation

$$I = \frac{2e}{\hbar} \frac{d\langle H_\Gamma \rangle}{d\Delta\phi}. \quad (64)$$

Notice that the fermion operators $d_{L,1\dots N-2}$ and $d_{R,2\dots N-1}$ essentially drop out from the problem—the full Hamiltonian separately conserves the fermion number for each of these states and they do not contribute to the Josephson current. Thus for the purposes of evaluating the current, the problem maps onto a simpler Hamiltonian involving only d_{end} , $d_{L,N-1}$, and $d_{R,1}$. In terms of $d_A = (d_{L,N-1} + d_{R,1})/\sqrt{2}$ and $d_B = (d_{L,N-1} - d_{R,1})/\sqrt{2}$, this effective Hamiltonian becomes

$$H_{\text{eff}} = t[(2d_A^\dagger d_A - 1) + (2d_B^\dagger d_B - 1)] + H_\Gamma, \quad (65)$$

where now

$$\begin{aligned} H_\Gamma &= \frac{\Gamma}{2} \{ C [(2d_{\text{end}}^\dagger d_{\text{end}} - 1) + (d_A^\dagger d_A - d_B^\dagger d_B)] \\ &\quad + C (d_A^\dagger d_B^\dagger + h.c.) + \sqrt{2} S [i d_{\text{end}}^\dagger (d_A^\dagger + d_B) + h.c.] \}. \end{aligned} \quad (66)$$

Applying degenerate perturbation theory to obtain the energies of the d_{end} , d_A , and d_B fermions to $O[(\Gamma/t)^2]$, we obtain

$$\begin{aligned} H_{\text{eff}} &\approx E_A \left(f_A^\dagger f_A - \frac{1}{2} \right) + E_B \left(f_B^\dagger f_B - \frac{1}{2} \right) \\ &\quad + E_{\text{end}} \left(f_{\text{end}}^\dagger f_{\text{end}} - \frac{1}{2} \right) \end{aligned} \quad (67)$$

The operators $f_{A/B/\text{end}}$ correspond to states that evolve from $d_{A/B/\text{end}}$ due to the tunneling perturbation. Their energies to the desired order are

$$E_{A/B} = 2t \pm \frac{\Gamma}{2} \cos(\Delta\phi/2) + \frac{\Gamma^2}{32t} [5 - 3 \cos \Delta\phi] \quad (68)$$

$$E_{\text{end}} = \Gamma \cos(\Delta\phi/2). \quad (69)$$

We can now evaluate the Josephson current in the ground state, as well as the excited state where the finite-energy quasiparticle formed from the fused Majoranas is occupied. Equations (64) and (67), along with the above energies, yield

$$I_\pm = \pm \frac{e\Gamma}{2\hbar} \sin(\Delta\phi/2) - \frac{3e\Gamma^2}{16\hbar t} \sin \Delta\phi, \quad (70)$$

where the $+/-$ sign corresponds to the current obtained when the f_{end} fermion is unoccupied/occupied. The second term represents the standard Josephson current that is 2π periodic in $\Delta\phi$. This contribution reflects Cooper-pair tunneling and thus arises at second-order in perturbation theory. More interestingly, the first term exhibits 4π periodicity and has a topological origin since it arises solely from the Majoranas fused at the junction. This contribution reflects a *first-order* process corresponding to single-electron tunneling, which is possible at zero bias because the Majoranas form a zero-energy state at the junction when $\Gamma = 0$.

It is interesting to observe from Eq. (68) that the $f_{A/B}$ fermions also pick up a first order correction to their energy from Γ . Thus one can view each of these states as individually contributing both 2π - and 4π -periodic Josephson currents. Their 4π -periodic contributions exactly cancel one another, however, so that only the fused Majoranas contribute to this effect. Mathematically, this can be understood from the particle/hole-symmetric spectrum of the Bogoliubov-de Gennes Hamiltonian in Eq. (65). This is plotted versus $\Delta\phi/(2\pi)$ in Fig. 9(b). Here only the solid lines denote physically distinct states since those with energy E and $-E$ are not independent. As one turns on the tunneling strength Γ from 0, the ordinary fermionic states that begin at energy $2t$ split with opposite sign at first order, and only yield a net change in energy at second order in Γ/t . Thus they contribute only to the usual 2π -periodic Josephson current. The state of affairs for the end state which begins at zero energy is very different—its energy also shifts at first order, but its ‘partner’ which shifts in the opposite direction does not represent a physically distinct state. It therefore produces an observable 4π -periodic Josephson current.

Finally, it is useful to ask whether the crossings in the spectrum of Fig. 9(b) at $\Delta\phi = \pi$ are stable. In the case of the ordinary $f_{A,B}$ quasiparticle states, they are certainly not. For instance, adding a weak superconducting pairing between $c_{L,N}$ and $c_{R,1}$ at the junction lifts the crossings near $E = \pm 2t$ in the figure. When this happens, there is no sense in which the bulk

quasiparticle states even individually contribute a 4π -periodic current. The crossing at $E = 0$, however, is stable provided the Majoranas at the outer ends of the wires do not overlap with those at the junction¹⁸. (The location of the crossing¹ though need not occur exactly at $\Delta\phi = \pi$). This can be understood as follows. As long as the occupation number of the fermion corresponding to the outer Majorana end states remains fixed, the ground states at $\Delta\phi = 0$ and $\Delta\phi = 2\pi$ have different fermion parity. In the former case $f_{\text{end}}^\dagger f_{\text{end}} = 0$ in the ground state while in the latter $f_{\text{end}}^\dagger f_{\text{end}} = 1$. If this crossing could be removed, then one would be able to adiabatically evolve $\Delta\phi$ from 0 to 2π while remaining in the ground state, but this can not happen unless the outer end Majoranas transfer a fermion to the junction. It is useful to keep this in mind when considering the left path of Fig. 4(b), where γ_2 crosses the junction. At fixed phase $\Delta\varphi^i \neq \pi$, the ground state is *always* accessible here, precisely because γ_2 overlaps with the fused Majoranas $\gamma_{3,4}$ at the junction during this process. However, when γ_2 resides at the far right end of the wire, then (neglecting residual overlap between the Majoranas) the ground state will no longer be accessible when the phase difference changes by 2π . This explains why the fractional Josephson current in Eq. (9) exhibits 2π periodicity in the initial phase difference $\Delta\varphi^i$, but 4π periodicity in $\Delta\varphi$.

Acknowledgments

We have benefited greatly from stimulating conversations with Sankar Das Sarma, Lukasz Fidkowski, Erik Henriksen, Alexei Kitaev, Patrick Lee, and Ady Stern. We also gratefully acknowledge support from the Lee A. DuBridge Foundation, ISF, BSF and DIP grants, Packard and Sloan fellowships, the Institute for Quantum Information under NSF grants PHY-0456720 and PHY-0803371, and the National Science Foundation through grant DMR-0529399.

¹ R. M. Lutchyn, J. D. Sau, and S. Das Sarma, arXiv:1002.4033 (unpublished).
² Y. Oreg, G. Refael, and F. von Oppen, arXiv:1003.1145 (unpublished).
³ A. Kitaev, Ann. Phys. **303**, 2 (2002).
⁴ S. Das Sarma, M. Freedman, and C. Nayak, Phys. Rev. Lett. **94**, 166802 (2005).
⁵ C. Nayak, S. H. Simon, A. Stern, M. Freedman, and S. Das Sarma, Rev. Mod. Phys. **80**, 1083 (2008).
⁶ N. Read and D. Green, Phys. Rev. B **61**, 10267 (2000).
⁷ D. A. Ivanov, Phys. Rev. Lett. **86**, 268 (2001).
⁸ G. Moore and N. Read, Nucl. Phys. B **360**, 362 (1991).
⁹ H. C. Choi, W. Kang, S. Das Sarma, L. N. Pfeiffer, and K. W. West, Phys. Rev. B **77**, 081301 (2008).
¹⁰ L. Fu and C. L. Kane, Phys. Rev. Lett. **100**, 096407 (2008).
¹¹ J. Linder, Y. Tanaka, T. Yokoyama, A. Sudbø, and N. Nagaosa, Phys. Rev. Lett. **104**, 067001 (2010).
¹² J. D. Sau, R. M. Lutchyn, S. Tewari, and S. Das Sarma, Phys. Rev.

Lett. **104**, 040502 (2010).
¹³ J. Alicea, Phys. Rev. B **81**, 125318 (2010).
¹⁴ M. Sato and S. Fujimoto, Phys. Rev. B **79**, 094504 (2009).
¹⁵ P. A. Lee, arXiv:0907.2681 (unpublished).
¹⁶ P. Ghosh, J. D. Sau, S. Tewari, and S. Das Sarma, arXiv:1006.3083 (unpublished).
¹⁷ X.-L. Qi, T. L. Hughes, and S.-C. Zhang, arXiv:1003.5448 (unpublished).
¹⁸ A. Y. Kitaev, Physics-Uspekhi **44**, 131 (2001).
¹⁹ M. Wimmer, A. R. Akhmerov, M. V. Medvedyeva, J. Tworzydło, and C. W. J. Beenakker, arXiv:1002.3570 (unpublished).
²⁰ L. Fu and C. L. Kane, Phys. Rev. B **79**, 161408(R) (2009).
²¹ F. Hassler, A. R. Akhmerov, C.-Y. Hou, and C. W. J. Beenakker, arXiv:1005.3423 (unpublished).
²² G. Dresselhaus, Phys. Rev. **100**, 580 (1955).
²³ Y. A. Bychkov and E. I. Rashba, J. Phys. C **17**, 6039 (1984).
²⁴ R. Winkler, *Spin-Orbit Coupling Effects in Two-Dimensional Electron and Hole Systems* (Springer, Berlin, 2003).

- ²⁵ A. Stern, F. von Oppen, and E. Mariani, *Phys. Rev. B* **70**, 205338 (2004).
- ²⁶ Y.-J. Doh, J. A. van Dam, A. L. Roest, E. P. A. M. Bakkers, L. P. Kouwenhoven, and S. De Franceschi, *Science* **309**, 272 (2005).
- ²⁷ M. Freedman, C. Nayak, and K. Walker, *Phys. Rev. B* **73**, 245307 (2006).
- ²⁸ P. Bonderson, S. Das Sarma, M. Freedman, and C. Nayak, arXiv:1003.2856 (unpublished).
- ²⁹ H.-J. Kwon, K. Sengupta, and V.M. Yakovenko, *Eur. Phys. J. B* **37**, 349 (2004).
- ³⁰ H.-J. Kwon, V. M. Yakovenko, and K. Sengupta, *Low Temp. Phys.* **30**, 613 (2004).